J Electroceram (2012) 28:202–207
DOI 10.1007/s10832-012-9708-5

Large signal response and harmonic distortion in piezoelectrics for SONAR transducers

Nevin P. Sherlock · Richard J. Meyer Jr.

Received: 19 October 2011 / Accepted: 7 March 2012 / Published online: 21 March 2012

Abstract Nonlinearity in the piezoelectric response limits the operating conditions of underwater transducers. In this work, the nonlinear effects are evaluated in terms of electrical current and induced strain as a function of drive level. Nonlinearity is further quantified within the active transduction material by evaluating the total harmonic distortion (THD) in the electromechanical response. Modified single crystals based on the binary lead magnesium niobate—lead titanate system were investigated. It is shown that single crystals show greater mechanical response and reduced THD, enabling operation at higher power levels. The performance of these single crystals is also compared to conventional high power lead zirconate titanate ceramics.

Keywords Piezoelectrics · Single crystals · PMNT · PMN-PT · Nonlinearity · Harmonic distortion

1 Introduction

Over the last decade, the use of ferroelectric single crystals over their polycrystalline counterparts has led to significant changes in the design and ultimate performance of many electromechanical devices. One such material is the binary relaxor ferroelectric lead magnesium niobate – lead titanate (PMNT) [1, 2]. PMNT crystals having the composition (1-x) $Pb(Mg_{1/3}Nb_{2/3})O_3 - x\ PbTiO_3$, with $0.28<x<0.35$, exhibit measured properties in excess of $K_{33}{}^{T}>7000\varepsilon_o$ (free permittivity), $d_{33}>2500$ pC/N (piezoelectric coefficient), and $k_{33}>0.92$ (electromechanical coupling coefficient) [3–5]. In particular, the high coupling coefficient leads to a wide frequency bandwidth in a device, which in-turn improves the resolution of the transducer. Increased resolution is of great interest in medical ultrasound transducers [6–8] as well as underwater SONAR projectors [9–11].

Although single crystal PMNT has shown great promise in improving the performance of broadband SONAR transducers, concerns have been raised relating to its performance under high power operation. The relatively low mechanical quality factor of single crystal PMNT (Q_M= 200) [12] relative to conventional high power lead zirconate titanate ceramics PZT4 and PZT8 (Q_M of 500 and 1000, respectively [13]) results in greater heat generation in PMNT devices due to mechanical losses [14]. Previous work has largely overcome the high mechanical losses with three independent types of modification to binary PMNT: the addition of $Pb(In_{1/2}Nb_{1/2})O_3$ or $Pb(Zr,Ti)O_3$ to form ternary PIMNT or PMNZT [15–17]; introduction of an internal bias by $Mn^{3,4+}$ doping [18–21]; and using the <011> crystallographic orientation in place of the conventional <001> direction [22, 23]. Furthermore it has been shown that modifications may be combined to further decrease the electromechanical losses while maintaining the high coupling coefficient of modified PMNT single crystals [12].

Modified PMNT single crystals show excellent potential for use in high power, broadband SONAR systems from the perspective of bandwidth, source level, and heat generation, but one issue which has received less attention is the harmonic distortion generated at high amplitude. Aurelle et al. has demonstrated significant harmonic distortion in Langevin transducers using Navy Type III ceramics [24]. Harmonic distortion presents a challenge for transducer and system designers in that it reduces the spectral content at the frequency of interest. More importantly, it may interfere with

N. P. Sherlock (✉) · R. J. Meyer Jr.
Applied Research Laboratory, The Pennsylvania State University,
P.O. Box 30, Mail Stop 2430A,
State College, PA 16804-0030, USA
e-mail: nevin.p.sherlock@gmail.com

complementary systems on a shared underwater platform [25]. In the case of a broadband SONAR system, harmonic distortion may even interfere with the sensor itself as the overtones may very well fall within the band of interest.

It has been shown that tonpilz transducers using modified PMNT single crystals generated total harmonic distortion (THD) in excess of 10 % in the acoustic source level under maximum operating conditions [26]. This is in contrast to conventional PZT4 tonpilz transducers, which exhibit approximately 3 % source level THD at the same source level. The origin of distortion in the active piezoelectric material is evident from the quasistatic strain response, as shown for baseline PMNT single crystal in Fig. 1. Note the change in slope as a function of electric field, which leads to distortion in the output mechanical response. The same nonlinear response can be seen in the polarization-field response [27].

Previous work has utilized a DC electrical bias in PMNT single crystal transducers to operate within a more stable window (i.e. less variation in slope), but the introduction of an external bias greatly increases the system cost and complexity [28]. Furthermore, the distortion measurements previously reported were made in a transducer, so while nonlinearities in the piezoelectric material were suspected as the primary contributor, that conclusion has not been proven. This work will therefore evaluate the electromechanical total harmonic distortion in modified single crystals and compare these values to conventional high power ceramics.

2 Experimental procedure

2.1 Materials of interest

Two single crystal compositions were selected for investigation: a binary PMNT composition ("base" PMNT) and a ternary PIMNT crystal, both from TRS Technologies, Inc. (State College, PA). The base PMNT was oriented along the conventional <001> crystallographic axis, while the PIMNT was modified to use the <011> direction. After crystal growth,

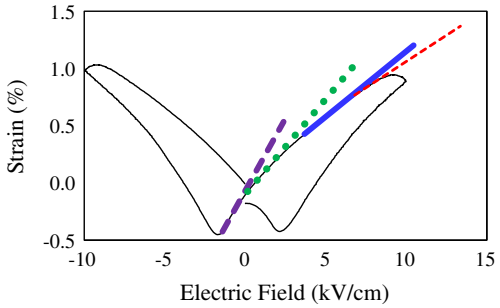

Fig. 1 (Color online) Strain-field response under bipolar drive in single crystal PMNT. Note the change in slope over the range of −2 kV/cm to 10 kV/cm, as indicated by line color, symbol, and thickness

33-mode bars were oriented using a Laue back-scatter diffractometer and cut to dimensions of 8 mm×1.5 mm×1.5 mm. Surfaces were polished to a 600 grit finish, and gold electrodes were sputter-coated on the bar ends. Bars were poled at room temperature using a field of 10-15 kV/cm (at least three times the coercive field) and aged for a minimum of 48 hours prior to electromechanical measurements.

Lead wires were attached to the electrodes using a conductive silver epoxy. Two electromechanically "hard" PZT ceramics were also selected for comparison to the single crystals. Electroded and poled 33-mode bars of PKI 402 (Navy Type I) and PKI 802 (Navy Type III) were obtained from Piezo Kinetics, Inc. (Bellefonte, PA). Dimensions of the ceramic bars were slightly larger than the single crystals (approximately 10 mm×2 mm×2 mm), but all samples maintained a length-to-width aspect ratio greater than 4:1.

2.2 Linear property measurements

Each sample was first characterized under linear conditions. The lead wires were clipped in a test fixture (Agilent 16047E, Santa Clara, CA) such that the bar was suspended in air, preventing any mechanical clamping effects. The room temperature capacitance and dissipation, Cp and tanδ, were measured at 1 kHz under 1 V drive using an impedance analyzer (Agilent 4184, Santa Clara, CA). The dielectric constant, K_{33}^{T}, was calculated as per the *IEEE Standard on Piezoelectricity* [29]. The same test setup was also used to measure the series and parallel resonance frequencies (f_s and f_p) and the half-power points (f_1 and f_2) about the series resonance peak. The 33-mode coupling coefficient (k_{33}) and mechanical quality factor (Q_M) were then calculated in accordance with the *IEEE Standard on Piezoelectricity* [29].

The piezoelectric d_{33} coefficient was measured under non-contact conditions using a Doppler laser vibrometer (OFV-505 laser unit and OFV-5000 laser control unit, Polytec Inc., Irvine, CA). A PXI-6115 data acquisition unit (National Instruments, Austin, TX) in combination with an EPA-104 amplifier (Piezo Systems, Inc., Woburn, MA) applied a pure tone sine wave at 1 kHz and 10 V_{pk} drive. The PXI-6115 unit also recorded the face vibration velocity, *vv*, which was used to calculate the quasistatic strain, *S*, according to

$$S = 2vv/\omega l \tag{1}$$

in which ω and l are the angular frequency and sample length, respectively. The factor of 2 in the numerator is because only one face of the bar was measured. From the calculated strain, and knowing the applied electric field, the piezoelectric coefficient was calculated from its definition as

$$d_{33} = S/E. \tag{2}$$

2.3 Large signal measurements

In order to prevent mechanical clamping effects during high drive measurements, each sample was again suspended by its lead wires in air. The PXI-6115 data acquisition unit was paired with an M8 high frequency amplifier (Instruments, Inc., San Diego, CA) to generate a pure tone, sinusoidal pulse at the resonance frequency. Due to transient ring-up effects, a Tukey window was used to gradually bring the sample into a steady state at resonance. Only the steady-state response was considered for harmonic distortion analysis. Measurements were repeated with increasing voltage until each bar fractured due to the induced mechanical stress. It should also be noted that the drive frequency was adjusted with increasing drive level, as the apparent resonance frequency is a function of amplitude due to the nonlinear tuning curve [30].

The PXI-6115 unit was also used to record the measured current waveform, as monitored by a VIT-13 variable input transformer (Instruments, Inc.), and vibration velocity waveform, as measured by the Polytec laser vibrometer. In all cases, a minimum of 300 cycles of steady-state current and vibration velocity response was captured for harmonic analysis. The dynamic strain was calculated from the measured vibration velocity by assuming a sinusoidal distribution of strain along the length of the bar. The maximum dynamic strain, located at the nodal plane of the bar, was calculated using Eq. (1) multiplied by a geometric factor of $\pi/2$.

The current and strain data was then analyzed using a fast Fourier transform to observe the spectral content, as depicted in Fig. 2. Total harmonic distortion in the current was calculated as

$$\mathrm{THD(I)} = \left(I_2{}^2 + I_3{}^2 + I_4{}^2\right)/I_1{}^2 \tag{3}$$

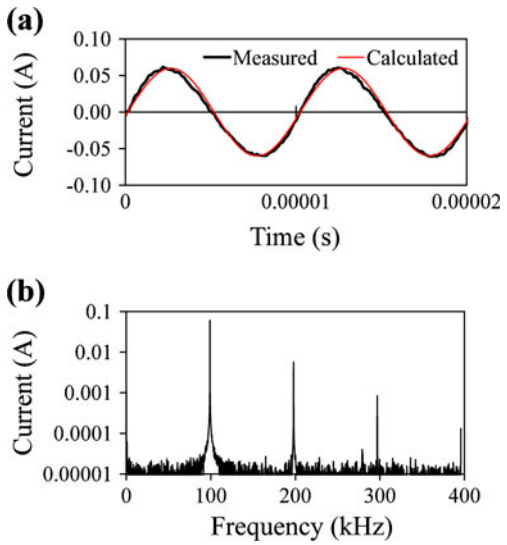

Fig. 2 (Color online) The *thick black line* shows measured current waveform (*top*) and spectrum (*bottom*) affected by harmonic distortion. A calculated pure tone sine wave is superimposed for comparison (*thin red line*)

in which I_1 represents the root mean square (RMS) current at the fundamental frequency and I_2, I_3, and I_4 represent the second, third, and fourth harmonics. This cutoff was chosen because higher order overtones were impossible to distinguish from baseline noise. The same technique was used to calculate THD in the applied voltage, designated THD(V), and in the mechanical strain response, designated THD(S).

3 Results and discussion

3.1 Linear property measurements

The electromechanical properties of modified single crystal (PMNT and PIMNT) and conventional ceramics (PKI 402 and 802) measured under linear conditions are shown in Table 1. The binary PMNT single crystal shows the greatest electromechanical response, as evidenced by the high $K_{33}{}^T$, d_{33}, and k_{33} values. It is interesting to note the measured quality factor of PMNT is much higher than previously reported in the literature, which is likely due to improvements in the crystal growth process and optimization of the PMN:PT ratio. The modified <011> PIMNT single crystal shows a lower response than base PMNT but also shows lower losses ($\tan\delta$=0.1 % and Q_M=850), which may enable greater performance in high power SONAR devices due to the lower heat generation. The PKI 402 and 802 ceramics also show low dielectric and mechanical losses, but demonstrate low piezoelectric response and coupling relative to the single crystals.

3.2 Large signal measurements

The peak electrical current and vibration velocity were measured as a function of applied voltage. In order to account for the sample dimensions, however, it is more convenient to plot these results with respect to electric field, current density, and mechanical strain. The current density induced at resonance is shown as a function of electric field in Fig. 3. Note the change in slope with increasing electric field, which is a reflection of increasing electrical impedance due to nonlinear softening. By

Table 1 Linear properties of single crystals and ceramics. Note the increasing hardness of <011> PIMNT relative to <001> PMNT and the greater electromechanical coupling and piezoelectric coefficient of <011> PIMNT relative to conventional high power ceramics

Material	$K_{33}{}^T$ (ε_o)	$\tan\delta$ (%)	k_{33}	d_{33} (pC/N)	Q_M
<001> PMNT	5250	0.3	0.88	1370	350
<011> PIMNT	2700	0.1	0.83	670	850
PKI 402	1550	0.2	0.63	295	410
PKI 802	1200	0.4	0.6	215	1060

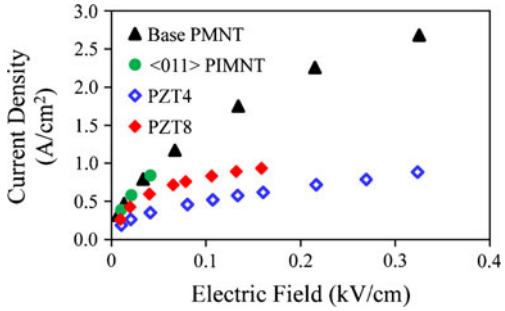

Fig. 3 (Color online) Measured current density at resonance as a function of applied electric field. Materials are designated by color and symbol

invoking the impedance analogy, the mechanical strain should be proportional to the current density (momentarily excluding nonlinear effects). This is confirmed in Fig. 4 in the trends of base PMNT, PKI 402, and PKI 802, but it is interesting to note the proportionally greater current density response relative to the dynamic strain in <011> PIMNT. The dynamic strain at resonance is proportional to the product $d_{33}{\cdot}Q_M$, which is consistent between the four materials between Table 1 and Fig. 4.

It is important to note that these four materials exhibit mechanical fracture at very different electric field levels, and there are three factors which must be considered. First, the elastic modulus varies between compositions, so a given vibration velocity will result in significantly different stress levels. Table 2 shows the strain and effective modulus (Y_R), as determined by the density and sound speed velocity, immediately prior to failure. The relationship

$$T = Y_R S \tag{4}$$

was then used to calculate the stress at failure. The difference in sample failure may also relate to the polycrystalline nature of the PKI 402 and 802. Grain boundaries within the material will arrest dislocation motion, leading to a higher failure stress. Finally, it was mentioned that the surfaces of these samples were only prepared to a 600 grit finish.

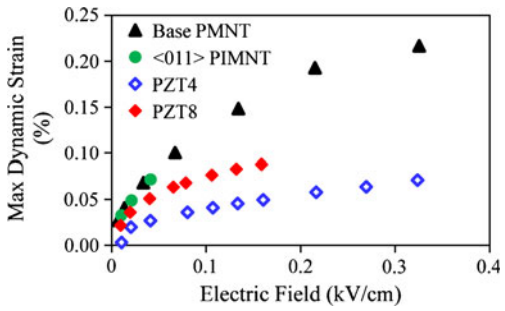

Fig. 4 (Color online) Dynamic strain located within the nodal plane of the sample at resonance as a function of applied electric field. The single crystal PMNT and PIMNT exhibit greater strain levels than the ceramics due to the greater $d_{33}{\cdot}Q_M$ products. Materials are designated by color and symbol

Table 2 Dynamic strain and stress during failure of piezoelectric samples. The measured dynamic strain S immediately prior to failure and the effective modulus Y_R determined from sample dimensions and resonance frequency were used to calculate the dynamic stress T at failure

Material	S (%)	Y_R (GPa)	T (MPa)
<001> PMNT	0.217	20.3	44.0
<011> PIMNT	0.072	39.3	28.4
PKI 402	0.068	64.7	50.8
PKI 802	0.084	74.6	62.7

Therefore, the distribution of large surface flaws near the center of the sample (i.e. highest stress region) may statistically dominate the failure strength of these materials. All three factors likely contributed to the low failure strain of <011> PIMNT compared to base PMNT, which was confirmed across multiple samples (not shown).

The total harmonic distortion in the applied voltage is shown in Fig. 5. Note that THD(V) is not an indication of distortion due to the piezoelectric effect, but is merely a measure of distortion in the amplifier and associated drive electronics. The reported values show THD(V) levels on the order of 0.3 % and independent of electric field, indicating high fidelity between the generated signal and the amplified waveform applied to the sample of interest. This baseline distortion must be considered when analyzing harmonic distortion in the current and mechanical response.

Figure 6 shows the harmonic distortion in the measured current. The current distortion is expressed as a function of an electrical parameter (current density), while the mechanical distortion is expressed as a function of a mechanical parameter (dynamic strain). Unlike the voltage distortion, which was constant as a function of increasing drive, the THD(I) increases significantly with increasing drive. The current shows an order of magnitude increase in distortion over THD(V), with the base PMNT exhibiting nearly 10 %

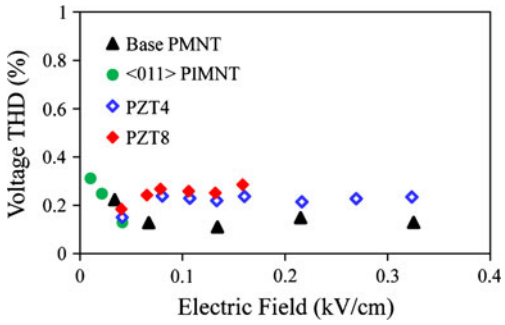

Fig. 5 (Color online) Total harmonic distortion in the applied voltage signal, with materials of interest designated by color and symbol. These THD(V) values are similar for all four samples because voltage distortion is largely a function of the amplifier and drive electronics, not the sample itself

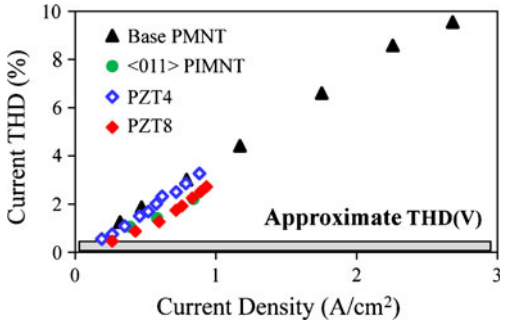

Fig. 6 (Color online) Total harmonic distortion in the measured current, with materials of interest designated by color and symbol. THD(I) is a strong function of the current density within the sample, and can reach 10 % in the case of PMNT

distortion prior to failure. It is also interesting to note that the base PMNT and PKI 402 show very similar distortion levels per unit of current density, while the electromechanically harder PKI 802 and <011> PIMNT show a slight decrease in THD(I). This may be due to the greater domain stability of PKI 802 and <011> PIMNT, and if so, it is likely that other piezoelectrics with low electromechanical losses (i.e. greater domain stability) would also show a decrease in THD(I) relative to "soft" piezoelectrics.

In contrast to the harmonic distortion in the electrical current, the four materials of interest show much lower distortion in the mechanical domain. Figure 7 demonstrates the THD(S) as a function of dynamic strain. Recall from Fig. 5 that a baseline distortion level of 0.3 % existed in the voltage signal applied to the sample, which in turn would pass through the measured velocity signal as well. This explains the relatively constant THD(S) of 0.2–0.3 % at strain levels less than 0.07 % in Fig. 7. The <011> PIMNT and PKI 402 mechanically fractured around this strain value, but the PMNT single crystal and PKI 802 show increasing harmonic distortion with strain as the drive level is further increased. Unlike the trend demonstrated in Fig. 6,

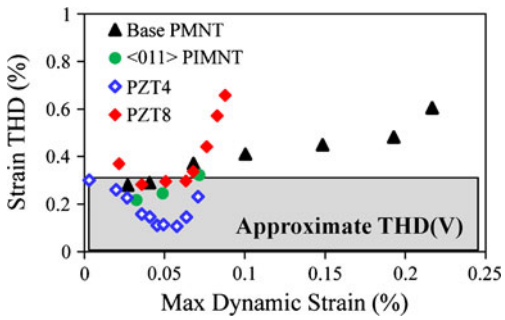

Fig. 7 (Color online) Total harmonic distortion in the mechanical response as determined by the measured vibration velocity, with materials of interest designated by color and symbol. At dynamic strain levels less than 0.07 %, the measured THD(S) is within the bounds of the harmonic distortion in the applied voltage. Higher strain levels result in mechanical distortion, but THD(S) is 5–10 times less than that observed in the current distortion THD(I)

the single crystal PMNT shows lower mechanical distortion than the PKI 802 under high strain conditions. This is interesting, as the electromechanically harder PKI 802 would be expected to show lower distortion levels, but recall that the PMNT exhibits much lower dynamic stress at a given strain due to the lower stiffness. As such, there would be a much greater parity in THD(S) if plotted as a function of dynamic stress instead of dynamic strain.

At high drive levels, the induced mechanical distortion increased beyond the baseline voltage distortion, but the maximum values of THD(S) were much less than the maximum current distortion. This trend is consistently shown in all four materials, with a maximum current distortion 5-10 times greater than the maximum mechanical distortion. In the case of a linear system, it would be expected that THD(I) and THD(S) should be equal simply by definition of the piezoelectric coefficient. The fact that a significant difference is observed in the harmonic distortion suggests a strong nonlinear component to the piezoelectric coefficient, and future work is needed to explore this relationship.

4 Conclusion

Four piezoelectric materials were investigated under large signal, nonlinear conditions. A binary PMNT single crystal was compared to a low loss <011> −oriented PIMNT crystal, and both single crystals were also compared to conventional high power PZT ceramics. The modified <011> PIMNT single crystal showed electromechanical losses comparable to the low loss PKI 802 ceramic, but maintained the high electromechanical coupling and piezoelectric coefficient characteristic to these single crystals. Both single crystals showed greater dynamic strain at resonance as a function of electric field, but mechanical fracture limited the maximum strain induced in the <011> PIMNT.

The total harmonic distortion was also measured in the electrical current and mechanical strain with increasing drive. It was confirmed that significant harmonic distortion was present at the material level due to nonlinearities in the electromechanical response. All four materials showed similar THD(I) levels at a given current density, although the distortion scaled roughly with the dielectric loss tanδ. This suggests that materials with greater domain stability may also show lower distortion in the electrical current. Although the harmonic distortion in the mechanical response was masked by the voltage THD at low strain levels, both the single crystal PMNT and PKI 802 exhibited mechanical distortion at high strain levels. In all four samples, total harmonic distortion in the electrical current was much greater than distortion in the mechanical strain, which suggests that there may be a nonlinear dependence of the piezoelectric coefficient as a function of drive. This possible

nonlinear relationship between current density and strain should be evaluated in additional piezoelectric materials, and future work to this effect is ongoing.

Acknowledgements The authors would like to thank Shujun Zhang and Tom Shrout at the Materials Research Laboratory for their collaboration and insights. Additional thanks to Jun Luo at TRS Technologies, Inc. for providing the single crystal samples. This work was supported by the Office of Naval Research (Arlington, VA), and the views contained do not represent official ONR policy or procedure.

References

1. S.-E. Park, T.R. Shrout, Ultrahigh strain and piezoelectric behavior in relaxor based ferroelectric single crystals. J. Appl. Phys. **82**(4), 1804–1811 (1997)
2. S.-E. Park, T.R. Shrout, Characteristics of relaxor-based piezoelectric single crystals for ultrasonic transducers. IEEE Trans. Ultrason. Ferroelectr. Freq. Control **44**(5), 1141–1147 (1997)
3. P. Han, W. Yan, J. Tian, X. Huang, H. Pan, Cut directions for the optimization of piezoelectric coefficients of lead magnesium titanate – lead titanate ferroelectric crystals. Appl. Phys. Lett. **86**, 052902 (2005)
4. S. Zhang, J. Luo, R. Xia, P.W. Rehrig, C.A. Randall, T.R. Shrout, Field-induced piezoelectric response in $Pb(Mg_{1/3}Nb_{2/3})O_3$ single crystals. Solid State Comm. **137**, 16–20 (2006)
5. K.K. Rajan, M. Shanthi, W.S. Chang, J. Lin, L.C. Lim, Dielectric and piezoelectric properties of [001] and [011]-poled relaxor ferroelectric pzn-pt and pmn-pt single crystals. Sensor Actuator A **133**, 110–116 (2007)
6. P.W. Rehrig, W.S. Hackenberger, X. Jiang, T.R. Shrout, S. Zhang, R. Speyer, "Status of piezoelectric single crystal growth for medical transducer applications," IEEE Ultrasonics Symposium, 766–769 (2003).
7. Y. Hosono, Y. Yamashita, Piezoelectric ceramics and single crystals for ultrasonic medical transducers. J. Electroceramics **17**(2), 577–583 (2006)
8. D.-G. Paeng, H.H. Kim, S.-G. Lee, S.M. Rhim, M.J. Choi, Fabrication of a 40 mhz single element ultrasonic transducer using a pmn-pt single crystal. Key Eng Mater **321–323**, 978–983 (2006)
9. R.J. Meyer, Jr., T.C. Montgomery, W.J. Hughes, Tonpilz transducers designed using single crystal piezoelectics. Proceedings of Oceans 2002 IEEE/MTS **4**, 2328–2333 (2002)
10. J.F. Tressler, T.R. Howarth, D. Huang, A comparison of the underwater acoustic performance of single crystal versus piezoelectric ceramic-based "cymbal" projectors. J. Acoust. Soc. Am. **119** (2), 879–889 (2006)
11. M.B. Moffett, H.C. Robinson, J.M. Powers, P.D. Baird, Single-crystal lead magnesium niobate – lead titanate (pmn/pt) as a broadband high power transduction material. J. Acoust. Soc. Am. **121**(5), 2591–2599 (2007)
12. N.P. Sherlock, S. Zhang, J. Luo, H.-Y. Lee, T.R. Shrout, R.J. Meyer Jr., Large signal electromechanical properties of low loss $(1\text{-}x)Pb(Mg_{1/3}Nb_{2/3})O_3 - xPbTiO_3$ single crystals. J. Appl. Phys. **107**, 074108 (2010)
13. B. Jaffe, W.R. Cook, H. Jaffe, *Piezoelectric Ceramics*, 2nd ed. Academic Press Limited (1990)
14. R.S. Woollett, "Power limitations of sonic transducers," IEEE Transactions on Sonics and Ultrasonics, **SU-15** (4) (1968)
15. S. Zhang, J. Luo, W. Hackenberger, T.R. Shrout, Characterization of $Pb(In_{1/2}Nb_{1/2})O_3 - Pb(Mg_{1/3}Nb_{2/3})O_3 - PbTiO_3$ ferroelectric crystal with enhanced phase transition temperatures. J. Appl. Phys. **104**, 064106 (2008)
16. V. Koval, C. Alemany, J. Briancin, H. Brunckova, Dielectric properties and phase transition behavior of xPMN – (1-x)PZT ceramic systems. J. Electroceramics **10**(1), 19–29 (2003)
17. S. Zhang, J. Luo, W. Hackenberger, N.P. Sherlock, R.J. Meyer Jr., T.R. Shrout, Electromechanical characterization of Pb(In1/2Nb1/2) O3 – Pb(Mg1/3Nb2/3)O3 – PbTiO3 crystals as a function of crystallographic orientation and temperature. J. Appl. Phys. **105**, 104506 (2009)
18. Y.-H. Chen, K. Uchino, D. Viehland, Substituent effects in 0.65Pb (Mg1/3Nb2/3)O3 – PbTiO3 piezoelectric ceramics. J. Electroceramics **6**(1), 13–19 (2001)
19. S. Priya, K. Uchino, Dielectric and piezoelectric properties of the mn-substituted $Pb(Zn_{1/3}Nb_{2/3})O_3 - PbTiO_3$ single crystal. J. Appl. Phys. **91**(7), 4515–4520 (2002)
20. S. Zhang, S.-M. Lee, D.-H. Kim, H.-Y. Lee, T.R. Shrout, Characterization of mn-modified $Pb(Mg_{1/3}Nb_{2/3})O_3 - PbZrO_3 - PbTiO_3$ single crystals for high power broad bandwidth transducers. Appl. Phys. Lett. **93**, 122908 (2008)
21. L. Liu, X. Li, X. Wu, Y. Wang, W. Di, D. Lin, X. Zhao, H. Luo, N. Neumann, Dielectric, ferroelectric, and pyroelectric characterization of mn-doped 0.74Pb(Mg1/3Nb2/3)O3–0.26PbTiO3 crystals for infrared detection applications. Appl. Phys. Lett. **95**, 192903 (2009)
22. S. Zhang, N.P. Sherlock, R.J. Meyer Jr., T.R. Shrout, Crystallographic dependence of loss in domain engineered relaxor-pt single crystals. Appl. Phys. Lett. **94**, 162906 (2009)
23. M. Shanthi, L.C. Lim, Electric-field and stress-induced R-O phase transformation in [001]-poled $Pb(Mg_{1/3}Nb_{2/3})O_3$ – (28–32)% $PbTiO_3$ single crystals of [100]-length cut. J. Appl. Phys. **106**, 114116 (2009)
24. N. Aurelle, D. Guyomar, C. Richard, P. Gonnard, L. Eyraud, Nonlinear behavior of an ultrasonic transducer. Ultrasonics **34**, 187–191 (1996)
25. C.H. Sherman, J.L. Butler, *Transducers and Arrays for Underwater Sound* (Springer, New York, NY, 2007)
26. N.P. Sherlock, *Relaxor-pt Single Crystals for Broad Bandwidth, High Power SONAR Projectors*. Ph.D. dissertation, The Pennsylvania State University, University Park, PA (2010)
27. X. Li, H. Luo, The growth and properties of relaxor-based ferroelectric single crystals. J. Am. Ceram. Soc. **93**(10), 2915–2928 (2010)
28. A. Amin, E. McLaughlin, H. Robinson, L. Ewart, Mechanical and thermal transitions in morphotropic pzn-pt and pmn-pt single crystals and their implication for sound projectors. IEEE Trans. Ultrason. Ferroelectrics Freq. Contr. **54**(6), 1090–1095 (2007)
29. *IEEE Standard on Piezoelectricity*, Standards Committee of the IEEE Ultrasonics, Ferroelectrics, and Frequency Control Society, New York, NY, USA (1987).
30. R. Perez, A. Albareda, Analysis of nonlinear effects in a piezoelectric resonator. J. Acoust. Soc. Am. **100**(6), 3561–3569 (1996)